## COMMUNICATION

Check for updates

# HV-CVD synthesis yielding B-doped SWCNTs with a constrained diameter distribution

Dido Denier van der Gon, [iD] *[a] Ramon Pinna-Brito,[a] Zhirui Liu, [iD] [b]
Cauê S. C. Nogueira,[c] Yuhei Miyauchi,[b] Thomas Pichler,[a] Oliver H. Heckl[a] and
Paola Ayala [iD] *[a]

Single-walled carbon nanotubes (SWCNTs) are among the most fundamental and revolutionary building blocks. Therefore, finding methods to tune their properties is highly desirable. Substitutional doping represents one feasible path toward this goal, in particular, for the semiconductors industry. In this work, it is shown how high-vacuum chemical vapor deposition (HV-CVD) enables the reliable and consistent growth of small-diameter B-doped SWCNTs with a set narrow diameter distribution over a 300 °C temperature window, independent from the composition of various tested catalysts. The synthesis parameters have only a minor influence on the diameter distribution. The method is rather feedstock and pressure dependent. This was explored using a wide range of catalysts, including both single- and multi-metal systems using different supports. These results demonstrate the versatility and robustness of HV-CVD with low-vapour pressure B-containing feedstocks as a path to nanotubes with defined and, with most catalysts, very narrow diameter distribution with minimal post-processing.

Carbon nanotubes (CNT) gained significant attention in the last decades owing to their outstanding physical properties.[1] Among their promising applications counts the integration as components for next-generation nano-electronic devices,[2] primarily because their structural, mechanical, and electronic characteristics are closely linked to the geometric distribution of the carbon (C) atoms along their tubular structure.[1] In particular, the electronic properties of a single-walled CNT (SWCNT) depend strongly on its diameter and chirality.[3] From this, it becomes clear that reliable techniques are needed to produce and sort nanotubes with specific characteristics. Among the strategies to tune the properties of SWCNTs is the controlled doping with heteroatoms such as boron (B) and nitrogen (N).[4–8] This offers a way to tailor the electronic properties of these materials. Theoretical studies on p-type doping in SWCNTs

using B atoms have focused on how they substitute C atoms within the lattice.[9–11] Given its one-electron deficiency compared to C, B substitution introduces localized states below the Fermi level $E_F$ and yields a shift toward a p-type semiconducting behavior.[9,12] It is expected that at low doping concentrations, the Fermi-level shifts down following a rigid band model, whereas at higher B-contents, different scenarios can be considered, such as the appearance of an acceptor state slightly above the valence band edge to the formation of hybrid C/B structures that do not comply a rigid band shift compared to their pristine counterparts.[9,10] Another possible scenario is the formation of B nanodomains along the tubular structures.[13,14] It is clear that in all these cases, B incorporation can modify not only the electronic but also the optical, vibrational,[12,15] thermal,[16] and catalytic[17] properties of SWCNTs. This explains studies towards applications in fields such as gas sensing,[18,19] solar cells,[20,21] batteries,[22] flexible devices,[23] and even superconducting materials.[14] B has been significantly less explored in applications over the past decades, compared to N doping in single-walled structures specifically.[6,7,21,24–26] The reasons behind this comprise practical difficulties with the different synthesis methods, and the attainable doping levels. A list of the available studies, to the best of our knowledge, on B-doped SWCNTs (CBx-SWNTs) can be found in the SI. Yet, their synthesis remains challenging in terms of yield and, to some extent in reproducibility. Laser ablation[27,28] and arc discharge[15] have been able to produce long CBx-SWNTs but the dopant concentration using these high temperature methods is very limited and B has hardly been detected.[29] Substitution reactions using SWCNTs and $B_2O_3$ have been used as alternative methods yielding CBx-SWNTs with B contents in the range of 1–3 at%.[16,23,30] Chemical vapor deposition (CVD), while more efficient for upscaling, presents experimental challenges due to the reactivity of B atoms with the reactors, unlike in standard protocols used for pristine SWCNTs. In this context, high-vacuum CVD (HV-CVD) methods employing low vapor pressure precursors have proven highly successful.[31,32] Still, even using low vapor pressures, only two liquid C/B feedstock types[31,33,34] and one solid precursor[35,36]

[a] *University of Vienna, Faculty of Physics, Boltzmanngasse 5, 1090, Vienna, Austria. E-mail: dido.denier.van.der.gon@univie.ac.at, paola.ayala@univie.ac.at*

[b] *Institute of Advanced Energy, Kyoto University, Uji, Kyoto, 611-0011, Japan*

[c] *The Polytechnic School, Arizona State University, Mesa, Arizona, 85212, USA*

have so far produced CBx-SWNTs with a clear substitutional B content. The CBx-SWNTs reported with these methods have been shown to grow within a small diameter range (when using liquid feedstocks)[37] and substitutional B contents below 1% have been revealed by XPS in non-purified samples,[38] although purification protocols for such materials have also been reported.[39] On the other hand, using a solid precursor in HV-CVD has shown to favor the B incorporation in the lattice with a record substitutional configuration.[35] Despite all efforts, the synthesis of CBx-SWNTs is evidently limited compared to the pristine material that can be easily produced nowadays with CVD-related methods. Different strategies have been developed to enhance yield and promote selectivity. Among others, the use of bi-metallic catalysts is a very efficient option for pristine tubes.[40–43] When using them, the diameter distribution of the resulting materials is typically broad for most hydro-carbon feedstocks used in CVD. However, while using various bi-metallic catalysts in our HV-CVD synthesis of CBx-SWNTs, the diameters remain narrowly distributed regardless the catalyst. In previous works, mainly iron-based catalysts had been proven effective.[32] Here we show that it is possible to use catalysts consisting of Fe, Fe–Co, Fe–Mo, Fe–Cu and Co–Mo supported in MgO and SiO$_2$. Remarkably, mostly small-diameter nanotubes grow across a temperature window of 300 °C. Moreover, the diameter distribution is constant and solely dependent on the feedstock.

The synthesis was carried out *via* the HV-CVD procedure[31,32,37] using triisopropyl borate (C$_9$H$_{21}$BO$_3$) as the carbon/boron feedstock. After the catalysts were mixed and calcined, they turned into homogeneous powders with metal loadings ranging from 1 to 2.5 wt% per metal (see further details in the SI). The HV-CVD process begins with the catalysts placed in the system and pumped to a base pressure of $10^{-6}$ mbar. They are subsequently reduced under a hydrogen flow while heating ($\sim$ 500 °C to 600 °C). After restoring the system to the base pressure, the temperature is increased (600–900 °C), at which point the catalyst is exposed to a continuous flow of C$_9$H$_{21}$BO$_3$ for 20 minutes. The system is then evacuated to the base pressure until cool.

The resulting samples were first inspected by Raman spectroscopy with a 633nm excitation wavelength (Fig. 1a). A multifrequency inspection was also carried out but we focus here on this laser line because it has revealed better the strongest resonant signals arising from larger diameter tubes, which are otherwise not revealed by optical absorption spectroscopy (OAS) when inspecting the overall diameter distribution (Fig. 1b). The spectra of the highest yield catalysts in Fig. 1a show that it is possible to produce efficiently single-walled material within a characteristic temperature window. However, from a combination of the results obtained from all the characterization techniques, it was clear that the main difference among the product from the different catalysts was the effective nanotube yield. Fig. 1a shows the Raman spectra of samples synthesized with different catalysts at 800 °C, since this temperature gives consistently high-yield. The $I_D/I_G$ ratio indicates that the highest structural quality is achieved with Fe, Fe–Co, and Fe–Mo-based catalysts. The RBM region reveals that the catalyst composition has a more pronounced effect on the diameter distribution than the synthesis temperature. This observation is
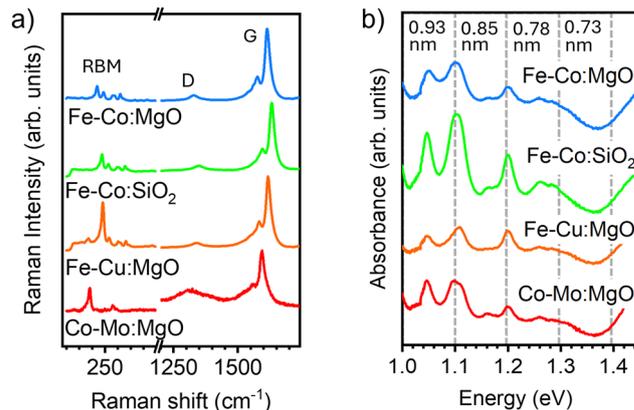


Fig. 1　Spectral response of material synthesized with different catalysts (a) Raman spectra the RBM, D and G band. (b) OAS in the $E_{11}$ region dispersed in 2% DOC. Dashed lines indicate energy ranges corresponding to specific average diameters, which are noted at the top.

consistent with previous reports linking nanotube diameter to the catalyst structure.[44] The smallest diameters are obtained using a silica support, in contrast to magnesium oxide, though at the expense of significantly lowering yield. Among the higher-yield catalysts (Fe, Fe–Co, Fe–Mo on magnesium oxide), nanotubes of similar diameters are in resonance with the same laser lines.[45] This suggests that the diameter growth range is similar for all samples, but the diameters out of the stable growth window can be tuned by changing the catalyst. The spectra in Fig. 2 correspond to material synthesized using an Fe–Co catalyst, which had overall the highest CBx-SWNT yield, and this material will be discussed further herein (additional spectra recorded from the other materials obtained from the highest yield catalyst can be found in the SI). We observed that nanotubes can be grown with temperatures as low as 600 °C but, from the $I_D/I_G$ ratio, 700 °C appears to be the onset for a more crystalline material, which attains its highest yield at 800 °C. The radial breathing mode (RBM) reveals, at first inspection, a consistent proportion of the same chiralities are
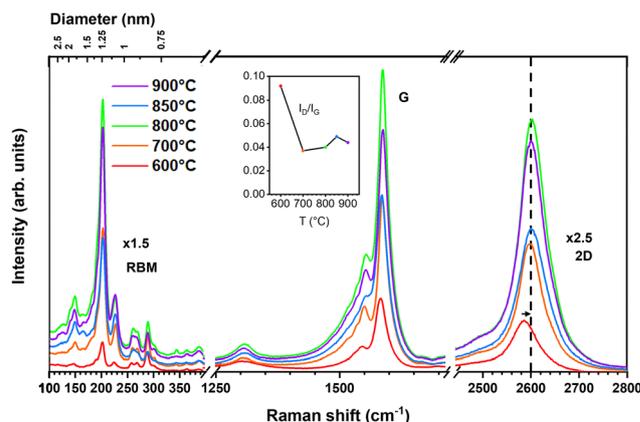


Fig. 2　Raman spectra of samples synthesized using the Fe–Co MgO catalyst at different temperatures measured using a 633 nm excitation wavelength. The RBM, D, G and 2D bands are shown. The $I_D/I_G$ ratio is indicated as inset.

present across the different synthesis temperatures.[45] An overall range of diameters between 0.7–1.8 nm can be identified but the highest Raman intensity still appears for diameters between 0.9 and 1.3 nm, as had been observed previously with Fe-based catalysts.[31,37] This narrow window of highest population of diameters appears to be very characteristic of $C_9H_{21}BO_3$. To gain a better overview of the diameter distribution it is necessary to look into the OAS, which provides a response of the diameters within a single measurement (see Fig. 1b). Unlike Raman spectroscopy, this technique is not resonance-dependent and therefore provides a more reliable estimate of diameter and chirality distributions. Prior to measurements, the samples were dispersed in 2 wt% deoxycholic acid sodium salt (DOC), centrifuged, and the supernatant was collected to remove catalyst residues, amorphous carbon, and other impurities. While differences in the diameter distributions between the samples are clearly visible, no strong dependence on size distribution is observed in these OAS measurements, in contrast to the results obtained from Raman spectroscopy with tubes of diameters ranging between 0.75 (6,5) and 0.97 (8,6), which is the range previously identified as feedstock dependent. Note that the transition energies here are not purely dependent on diameter (without further considerations), thus only a distribution has been taken from the data rather than the exact diameters present in the sample. The OAS spectra of material made using the Fe-Co:MgO catalyst reveal consistent growth from 600 to 900 °C. The absorbance spectra in the $E_{11}$ range for different temperatures are shown in the inset of Fig. 3. Here, it can be observed that the absorbance broadens towards lower energies, suggesting the presence of larger diameters for higher synthesis temperatures, which is to some extent in agreement with the Raman measurements. Note that the samples are not purified so the intensities cannot be directly related to sample quality, as they are influenced by varying optical densities due to differences in the amount of starting materials and the residual catalyst. We have applied a short cleaning procedure to discern the effect of temperature (or catalyst) on the synthesis process, without introducing variability from different purification methods, which might be more chirality dependent. Although different surfactants exhibit varying affinities for specific diameter ranges of nanotubes,[46] this has not been accounted for in the present study. Nevertheless, DOC is among the most widely used surfactants for dispersing nanotubes across a broad diameter range.

All OAS were fitted with Voigt functions to obtain the absorption energy and abundance of the different tubes present. Using the approximate $\frac{1}{d}$ relationship between diameter and absorbance in the $E_{11}$ region of the nanotubes, we plotted the abundances per sample as a function of diameter for the distributions of the synthesis at different temperatures, as shown in the main panel of Fig. 3. It is important to emphasize that due to the absorption of water, the absorbance below 1 eV cannot be determined and larger diameter tubes cannot be identified. Therefore, complementing the optical absorbance data with the Raman measurements performed earlier, we obtain a reliable picture of the overall diameter distribution of the sample. Fig. 3 shows that the median diameter remains constant at 0.85 nm for synthesis up to 850 °C. At higher temperatures (900 °C), however, the median as well as the average shifts toward larger diameters, and the quality of the material deteriorates. Within the optimal synthesis range of 700–850 °C for this system, as determined from the $I_D/I_G$ ratio of the Raman spectra, the distribution remains nearly unchanged. This indicates that in the optimal range the synthesis process is largely temperature independent. Similar results are obtained when using different catalysts (Fig. 1b) although the changes in the distribution are slightly more pronounced. When varying the catalyst, the distribution remains unchanged while the median diameter shifts. In contrast, replacing a bi-metallic catalyst containing iron with one without it, results in the same median diameter but shifts the distribution toward larger diameters. These observations indicate that although small variations can be induced through changes in synthesis parameters, the overall outcome of the synthesis remains largely consistent even under substantial modifications. As a result, we are able to take advantage of the enhanced versatility of the method, which consistently yields small-diameter tubes with a narrow diameter distribution. At the same time, the well-known and well-understood electronic properties of pure C nanotubes are preserved. In addition to demonstrating robustness with respect to temperature and catalyst variations, the reproducibility of the synthesis was evaluated. With this purpose, several experiments were carried out under the same condition and the resulting nanotubes were measured also under identical conditions. From the Raman measurements, we could observe that the RBMs remained practically invariant (including their intensities), while the $I_D/I_G$ ratio varies by no more than 0.02 units between experiments (see SI). This clearly proves the reproducibility of our results and the robustness of the method.

Photoluminescence (PL) measurements were performed to further evaluate the optical properties of the CBx-SWNTs, as light emission plays a crucial role in many potential applications. A representative PL excitation map of a sample synthesized at
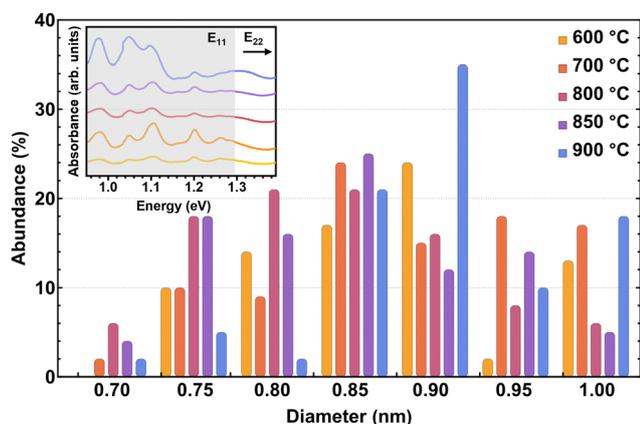


Fig. 3 Tube diameter distribution estimated from OAS on samples of made with a Fe–Co:MgO co-catalyst using 600 to 900 °C. The full OAS in the $E_{11}$ region of CBx-SWNT dispersed in DOC2% is shown as inset.
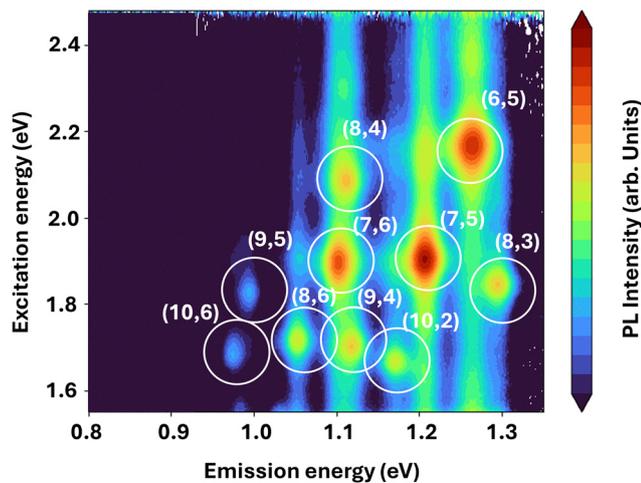
Fig. 4 PL excitation map of CBx-SWNT synthesized at 800 °C (Fe–Co co-catalyst on MgO), dispersed in water with DOC. PL intensity is shown on a logarithmic scale to highlight the different chiralities present in the sample, which are identified and circled.

800 °C using the Fe–Co on MgO catalyst and dispersed in water with DOC is shown in Fig. 4. The PL intensity is plotted on a logarithmic scale to emphasize the different chiralities present in the sample, which are circled and labeled for clarity. The observed diameter distribution again remains narrow, ranging from approximately 0.75 nm (6,5) to 1.1 nm (10,6). Also here, the larger diameter tubes which, based on the Raman spectra, are present in the sample are again not visible due to the absorbance of the emitted light by the water solution. These results confirm the presence of well-defined chiralities and illustrate the potential of such samples for optoelectronic and bio-imaging applications.

Summarizing, the low vapour pressure of $C_9H_{21}BO_3$ combined with a HV-CVD procedure enables a reliable and consistent growth pathway for CBx-SWNTs within a highly populated and constrained thin tube-diameter range. Independent of the catalyst used, a wide temperature range from 700 to 900 °C allows the growth of material. Raman and absorbance spectroscopy reveal that variations in synthesis parameters have only a minor impact on the resulting diameter distribution. Furthermore, a persisting morphology can be identified using a wide range of catalysts. Their composition can affect the overall sample quality but the presence of tubes within the diameter range between 0.9 and 1.3 nm remains present almost unaltered while using the same feedstock. In addition to the robustness under varying synthesis parameters, the results are highly reproducible under identical conditions. These results highlight the versatility and robustness of this HV-CVD approach. Given its simplicity, the weak parameter dependence, and the scale-up potential, this approach represents the possibility of efficiently enabling their applicability.

D. M. Denier van der Gon: data curation, analysis, investigation, methodology, visualization, writing. R. Pinna Brito: data curation, investigation. Z. Liu: methodology, investigation. C.S.C. Nogueira: data curation, investigation. Y. Miyauchi: supervision, review & editing. T. Pichler: review & editing. O.H. Heckl: supervision, review & editing. P. Ayala: conceptualization, methodology, supervision, writing – review & editing.

## Conflicts of interest

There are no conflicts to declare.

## Data availability

The data supporting this article have been included as part of the supplementary information (SI), which includes all the original full Raman spectra recorded for all reported samples. Tables containing information from previous publications are referenced in the supplementary information. No special software has been used for the data obtained in this manuscript. Therefore, no software or code have been included. See DOI: https://doi.org/10.1039/d5cc07030a.

## Acknowledgements

## References

1 J. C. Charlier, X. Blase and S. Roche, *Rev. Mod. Phys.*, 2007, **79**, 677.
2 P. Avouris and J. Chen, *Mater. Today*, 2006, **9**, 46.
3 R. Saito, G. Dresselhaus and M. S. Dresselhaus, *Physical Properties of Carbon Nanotubes*, Imperial College Press, London, 1998, vol. 76.
4 P. Ayala, R. Arenal, A. Loiseau, A. Rubio and T. Pichler, *Rev. Mod. Phys.*, 2010, **82**, 1843.
5 O. Stephan, P. M. Ajayan, C. Colliex, P. Redlich, J. M. Lambert, P. Bernier and P. Lefin, *Science*, 1994, **266**, 1683.
6 M. Terrones, A. Jorio, M. Endo, A. M. Rao, Y. A. Kim, T. Hayashi, H. Terrones, J. C. Charlier, G. Dresselhaus and M. S. Dresselhaus, *Mater. Today*, 2004, **7**, 30.
7 A. K. Thakur, K. Kurtyka, M. Majumder, X. Yang, H. Q. Ta, A. Bachmatiuk, L. Liu, B. Trzebicka and M. H. Rummeli, *Adv. Mater. Interfaces*, 2022, **9**, 2101964.
8 A. Karagianni, N. G. Tsierkezos, A. Ntziouni, M. Terrones and K. V. Kordatos, *Carbon*, 2026, **246**, 120832.
9 L. Wirtz and A. Rubio, *AIP Conf. Proc.*, 2003, **685**, 402.
10 J. Y. Yi and J. Bernholc, *Phys. Rev. B: Condens. Matter Mater. Phys.*, 1993, **47**, 1708.
11 T. Koretsune and S. Saito, *Sci. Technol. Adv. Mater.*, 2009, **9**, 044203.
12 I. O. Maciel, N. Anderson, M. A. Pimenta, A. Hartschuh, H. Qian, M. Terrones, H. Terrones, J. Campos-Delgado, A. M. Rao, L. Novotny and A. Jorio, *Nat. Mater.*, 2008, **7**, 878.
13 D. L. Carroll, P. Redlich, X. Blase, J. C. Charlier, S. Curran, S. Roth, P. M. Ajayan and M. Rühle, *Phys. Rev. Lett.*, 1998, **81**, 2332.
14 N. Murata, J. Haruyama, J. Reppert, A. M. Rao, T. Koretsune, S. Saito, M. Matsudaira and Y. Yagi, *Phys. Rev. Lett.*, 2008, **101**, 027002.
15 K. McGuire, N. Gothard, P. L. Gai, M. S. Dresselhaus, G. Sumanasekera and A. M. Rao, *Carbon*, 2005, **43**, 219.
16 W. H. Chiang, Y. Iihara, W. T. Li, C. Y. Hsieh, S. C. Lo, C. Goto, A. Tani, T. Kawai and Y. Nonoguchi, *ACS Appl. Mater. Interfaces*, 2019, **11**, 7235.

17 Y. Lin, S. Wu, W. Shi, B. Zhang, J. Wang, Y. A. Kim, M. Endo and D. S. Su, *Chem. Commun.*, 2015, **51**, 13086.

18 M. M. Rana, D. S. Ibrahim, M. R. Asyraf, S. Jarin and A. Tomal, *Sens. Rev.*, 2017, **37**, 127.

19 W. An and C. H. Turner, *Chem. Phys. Lett.*, 2009, **482**, 274.

20 W. Li, S. Zhang, Q. Chen and Q. Zhong, *Catal. Sci. Technol.*, 2021, **11**, 2745.

21 X. Zheng, H. Chen, Q. Li, Y. Yang, Z. Wei, Y. Bai, Y. Qiu, D. Zhou, K. S. Wong and S. Yang, *Nano Lett.*, 2017, **17**, 2496.

22 I. Mukhopadhyay, N. Hoshino, S. Kawasaki, F. Okino, W. K. Hsu and H. Touhara, *J. Electrochem. Soc.*, 2002, **149**, A39.

23 Y. Liu, V. Khavrus, T. Lehmann, H. L. Yang, L. Stepien, M. Greifzu, S. Oswald, T. Gemming, V. Bezugly and G. Cuniberti, *ACS Appl. Energy Mater.*, 2020, **3**, 2556.

24 P. Ayala, R. Arenal, M. Rümmeli, A. Rubio and T. Pichler, *Carbon*, 2010, **48**, 575.

25 S. V. Sawant, A. W. Patwardhan, J. B. Joshi and K. Dasgupta, *Chem. Eng. J.*, 2022, **427**, 131616.

26 W. Dai, R. Wang, Z. Chen, S. Deng, C. Huang, W. Luo and H. Chen, *J. Mater. Chem. A*, 2023, **11**, 7584.

27 J. L. Blackburn, Y. Yan, C. Engtrakul, P. A. Parilla, K. Jones, T. Gennett, A. C. Dillon and M. J. Heben, *Chem. Mater.*, 2006, **18**, 2558.

28 L. S. Panchakarla, A. Govindaraj and C. N. Rao, *Inorg. Chim. Acta*, 2010, **363**, 4163.

29 B. Anand, R. Podila, P. Ayala, L. Oliveira, R. Philip, S. S. Sankara Sai, A. A. Zakhidov and A. M. Rao, *Nanoscale*, 2013, **5**, 7271.

30 E. Borowiak-Palen, T. Pichler, A. Graff, R. J. Kalenczuk, M. Knupfer and J. Fink, *Carbon*, 2004, **42**, 1123–1126.

31 P. Ayala, W. Plank, A. Grüneis, E. I. Kauppinen, M. H. Rümmeli, H. Kuzmany and T. Pichler, *J. Mater. Chem.*, 2008, **18**, 5676.

32 S. Daothong, J. Parjanne, E. I. Kauppinen, M. Valkeapää, T. Pichler, P. Singjai and P. Ayala, *Phys. Status Solidi B*, 2009, **246**, 2518.

33 P. Ayala, M. H. Rümmeli, T. Gemming, E. Kauppinen, H. Kuzmany and T. Pichler, *Phys. Status Solidi B*, 2008, **245**, 1935.

34 F. H. Monteiro, D. G. Larrude, M. E. Maia Da Costa, L. A. Terrazos, R. B. Capaz and F. L. Freire, *J. Phys. Chem. C*, 2012, **116**, 3281.

35 C. Reinoso, L. Shi, O. Domanov, P. Rohringer, T. Pichler and P. Ayala, *Carbon*, 2018, **140**, 259.

36 C. Reinoso, C. Berkmann, L. Shi, A. Debut, K. Yanagi, T. Pichler and P. Ayala, *ACS Omega*, 2019, **4**, 1941.

37 G. Ruiz-Soria, S. Daothong, T. Pichler and P. Ayala, *Phys. Status Solidi B*, 2012, **249**, 2469.

38 P. Ayala, J. Reppert, M. Grobosch, M. Knupfer, T. Pichler and A. M. Rao, *Appl. Phys. Lett.*, 2010, **96**, 183110.

39 G. Ruiz-Soria, P. Ayala, S. Puchegger, H. Kataura, K. Yanagi and T. Pichler, *Phys. Status Solidi B*, 2011, **248**, 2504.

40 S. Maruyama, R. Kojima, Y. Miyauchi, S. Chiashi and M. Kohno, *Chem. Phys. Lett.*, 2002, **360**, 229.

41 X.-D. Wang, K. Vinodgopal and G.-P. Dai, Synthesis of Carbon Nanotubes by Catalytic Chemical Vapor Deposition, Perspective of Carbon Nanotubes, 2019.

42 Y. Yuan, B. Lamichhane, W. N. Porter, S. Hwang, L. Ma, D. Yang, A. Tayal, N. S. Marinkovic, S. Kattel and J. G. Chen, *Chem. Catal.*, 2025, **5**, 101428.

43 Q. Jiang, Y. Wu, F. Wang, P. Zhu, R. Li, Y. Zhao, Y. Huang, X. Wu, S. Zhao, Y. Li, B. Wang, D. Gao and R. Zhang, *Adv. Mater.*, 2024, **36**, 2402257.

44 A. C. Dupuis, *Prog. Mater. Sci.*, 2005, **50**, 929.

45 C. Fantini, A. Jorio, M. Souza, M. S. Strano, M. S. Dresselhaus and M. A. Pimenta, *Phys. Rev. Lett.*, 2004, **93**, 147406.

46 H. B. Yang, L. Neal, E. E. Flores, A. Adronov and N. Y. Kim, *J. Surfactants Deterg.*, 2023, **26**, 607.